STRESS SEPARATION IN DIGITAL PHOTOELASTICITY PART B - WHOLE FIELD EVALUATION OF STRESS COMPONENTS

M. Ramji* and K. Ramesh**

Abstract

In photoelasticity, the method of obtaining the individual values of principal stresses/normal stresses separately is referred to as stress separation. For stress separation, one needs the value of fringe order and the isoclinic angle free of noise over the domain. With improved data acquisition and smoothing methodologies, it has now become possible to get accurate and smooth variation of the fringe order and the isoclinic value over the domain. This has been discussed in detail in Part-A of this article. Shear difference is one of the widely used techniques for stress separation in photoelasticity. Though it is a line byline technique, a whole field evaluation of stress separation using this technique and its representation is shown in this paper. It is observed that spikes in isoclinic values lead to streak formation in the whole field representation of separated stress components. The use of outlier algorithm for smoothing isoclinic and isochromatic data has removed these streaks and has also greatly improved the accuracy of the separated stress components. The various issues related to digital implementation such as boundary pixel identification, grids for accommodating the various boundaries etc. are given in the Appendix. Performance of the methodology is verified for simply and multiply connected objects. The models are subjected to moderate loads to have sufficient isochromatic-isoclinic interaction. The stress components obtained are smoothed with the outlier algorithm for improved accuracy. Whole field separated stress values are obtained for the domains considered.

Introduction

The recent developments in digital image processing have given birth to a separate branch of photoelasticity called *digital photoelasticity* [1]. It is well known that photoelasticity directly gives only the principal stress difference and in-plane shear stress. In certain class of problems, it is necessary to find individual stress components over the domain. To carry out this, auxiliary methods in conjunction with photoelasticity are used. Auxiliary methods can be additional experiments, numerical methods, integration of equilibrium equations [2] etc. In the case of additional experiments, oblique incidence [3, 4], holophotoelasticity [5], interferometry [6, 7] or thermophotoelasticity [8] have been used. Nurse [9] proposed a path - independent stress separation technique using fast Fourier transforms. Ramesh and Mangal [10] extended the use of oblique incidence approach for whole field stress separation by taking advantage of the developments in digital photoelasticity. They proposed a technique that use only isochromatic data from a few angles of oblique incidence. Stress separation is done in a least squares sense from these. A simulation study by them showed that the technique demanded a six to eight digit accuracy of isochromatic data which is beyond the purview of any of the available digital photoelastic techniques today. The technique of holophotoelasticity, interferometry and thermophotoelasticity directly give the whole field values of the sum of the principal stresses. Thus in conjunction with photoelasticity, one gets separated principal stress values. The main drawback in these approaches is that they require additional experimental set up other than photoelasticity. The use of numerical methods such as finite element [11, 12] or boundary element [13-15] in conjunction with photoelasticity for stress separation are called hybrid techniques. Separation of stresses is accomplished by using the numerical solution of sum of principal stresses [16-18] and photoelastic data.

The shear difference method is the most commonly used technique because of its simplicity and versatility [19]. It is based upon the integration of equilibrium equations. Case and Barkoff [20] first developed a computer

* Research Scholar ** Professor and Head
Department of Applied Mechanics, Indian Institute of Technology Madras, Chennai-600 036, India; Email : kramesh@iitm.ac.in
Manuscript received on 22 May 2007; Paper reviewed, revised and accepted on 16 Nov 2007

assisted programming for the implementation of the conventional shear difference. Later, Trebuna [21] implemented both the conventional and Tesar's modified shear difference technique for separation of stress components in reflection photoelasticity using a PC. There have been limited studies on the shear difference technique in digital photoelasticity too [22, 23]. Haake et. al [22] obtained photoelastic data using their six step phase shifting algorithm [24] and using this evaluated stress components for 2-D and 3-D problems by conventional shear difference technique. Xue-Feng Yao et. al [23] showed the use of conventional shear difference for stress separation along a line including stress concentration zones. Although, these works presented initial studies on using digital photoelastic methods for stress separation, the various issues regarding the digital implementation of the shear difference technique and the influence of error in isoclinic or isochromatic data on stress separation has not been studied. Further, the presentation of separated stress components confined to selected lines only.

A digital implementation of the shear difference technique for whole field stress separation of 2-D problems of any geometry is presented in this paper. For stress separation using the shear difference technique, one needs both isochromatics and isoclinics free of noise. A detailed procedure discussed in Part-A of the paper is used for evaluating the isoclinic and isochromatic data free of noise and spikes. In order to minimize the error in stress separation, Tesar's modification of the shear difference scheme is employed. Firstly, the shear difference algorithm is validated for the benchmark problem of a disk under diametral compression which is a simply connected body. Then it is extended for handling the multiply connected model of a ring subjected to internal pressure. Influence of noise on isochromatic and isoclinic data on the accuracy of the separated stress components is also discussed. The various issues related to digital implementation such as boundary pixel identification, modified boundary grids for implementing the shear difference algorithm etc. are presented in an Appendix. For completeness the methodology of shear difference is presented briefly.

Stress Separation by Shear Difference Technique

In the absence of body forces, the equation of equilibrium when applied to the problem of plane stress is

$$\frac{\partial \sigma_x}{\partial x} + \frac{\partial \tau_{yx}}{\partial y} = 0 \tag{1}$$

If Eq. (1) is numerically integrated using a finite difference approximation, one gets

$$(\sigma_x)_j = (\sigma_x)_i - \sum_i^j \frac{\Delta \tau_{yx}}{\Delta y} \Delta x \tag{2}$$

and τ_{xy} is directly obtained from photoelastic data as

$$\tau_{xy} = \frac{(\sigma_1 - \sigma_2)}{2} \sin 2\theta = \frac{N F_\sigma}{2h} \sin 2\theta \tag{3}$$

Using Eq. (2), stress separation can be done along lines parallel to x-axis. The $(\sigma_x)_i$ in Eq. (2) is the initial value at the start of the integration procedure (usually a free boundary, Fig.1) and $\Delta \tau_{xy}/\Delta y$ is evaluated for increments of Δx. One of the main sources of error accumulation in shear difference technique is in the calculation of the shear slope ($\Delta \tau_{xy}/\Delta y$). Vadovic [25] has shown that Tesar's modified shear difference equation contains lesser error than that of the conventional shear difference scheme. Tesar's modified shear difference equation is given as [25]

$$(\sigma_x)_j = (\sigma_x)_i - \sum_i^j \frac{\Delta(\sigma_1 - \sigma_2)}{\Delta y} \frac{1}{2} \sin 2\theta \Delta x - \sum_i^j (\sigma_1 - \sigma_2) \cos 2\theta \frac{\Delta \theta}{\Delta y} \Delta x \tag{4}$$

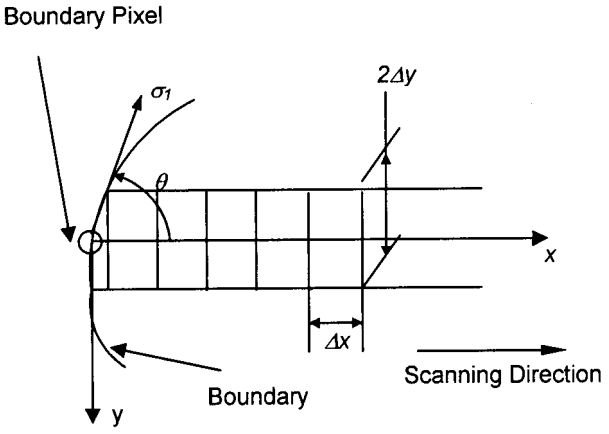

Fig.1 Figure showing the grid needed for employing the shear difference method. The free boundary stress component is also shown.

After calculating σ_x at a point in the grid, σ_y can be evaluated as

$$(\sigma_y)_j = (\sigma_x)_j - \frac{N F_\sigma}{h} \cos 2\theta \quad (5)$$

Whole Field Evaluation of Stress Components

Implementation of the stress separation method requires the formation of a grid consisting of three adjacent rows of pixels with the central row being the row of interest i.e., the row corresponding to each pixel of which, the stress components in the *x* and *y* directions are calculated. The line of interest is denoted as the 'central line', a line above the line of interest is designated as the 'top line' and a line below the line of interest is designated as the 'bottom line'. The grid structure is shown in Fig.1. Even though, physically the model may have a curved boundary, digitally it has to be looked at as an assembly of straight lines. The various possible cases of boundaries that need to be considered for performing the shear difference integration is shown in Appendix.

To apply the shear difference technique, one needs isochromatic and isoclinic data at each pixel along the three lines, on the line of interest and one each on the above and below the line of interest (See Eq. (4)). Also one needs the boundary value of *N* and θ in the line of interest while carrying out the shear difference algorithm.

Usually, phase shifting techniques (PST) for data acquisition gives the photoelastic data as an array. A proper data structure is needed for retrieving the requisite data for the implementation of the algorithm. The details of the data management are explained in the Appendix. Using the bright field image of the problem domain, primary boundary file (**.ybn*) is generated. Then using the primary boundary information, the modified boundary information (**.mbn*) as mentioned in the Appendix is constructed. Using this file, the fringe order and the isoclinic values at every pixel over the chosen model domain is obtained and written in a file (**.shd*). This **.shd* file forms the main input file for stress separation.

The stress separation algorithm is carried out row-wise horizontally starting from the boundary pixel. From the **.mbn* file, one gets the line number and the starting pixel number. Based on the starting pixel number, pixel coordinates, isochromatic and isoclinic data are read from the **.shd* file. At every pixel, τ_{xy} is calculated directly using the photoelastic data, followed by σ_x and then σ_y using the shear difference scheme. The process is repeated for all the lines pixel-wise within the model domain. The boundary grid structure for each line will be identified based on the pixel co-ordinates of three adjacent lines and the corresponding shear difference equation will be selected for stress separation. The separated stress values along with the coordinate values pixel-wise are printed in a file row-wise (**.sep*). Thus, individual stress values for all the pixels within the model domain are available in this file.

Evaluation of Stress Components Using Theoretically Generated Data

For illustrating the implementation of the shear difference algorithm, the problem of a disk under diametral compression used in Part-A (dia = 60 mm, thickness = 6.1 mm, Fsigma = 11 N/mm/fringe) is chosen. In view of symmetry, only one quarter of the disk is analysed. Fig.2a and 2b show the contours of isochromatics ($\sigma_1 - \sigma_2$) and isoclinics (in steps of 10°) obtained using the elasticity solution [29]. From the data of **.ybn* file, **.mbn* file is created and the **.shd* file file is then created to facilitate applying the stress separation algorithm. Following the methodology mentioned in the Appendix, the stress components are separated. In order to easily visualize the whole field representation of the separated stress components, the following approach is adopted. In this, following the approach of stress-optic law, for plotting σ_x stress

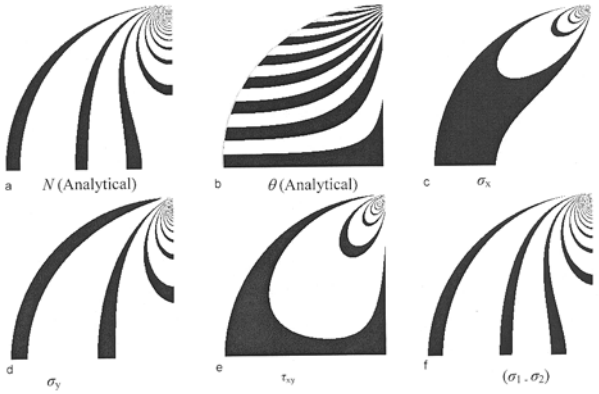

Fig.2

Pseudo fringe contours showing variation of stresses for a problem of disk under diametral compression determined by shear difference technique using theoretical data along with the photoelastic parameter. (a) N (b) θ (isoclinic plot in steps of 10°) (c) σ_x (d) σ_y (e) τ_y (f) dark field isochromatic (using separated stress components)

component, the value of the fringe order ($N_{\sigma x}$) is obtained by

$$N_{\sigma x} \quad \frac{\sigma_x h}{F_\sigma} \tag{6}$$

On similar lines, one can also plot σ_y and τ_{xy} pseudo fringe contours. Figs.2c-e show the pseudo fringe contours of σ_x, σ_y and τ_{xy} obtained using the shear difference scheme. Fig. 2f shows the isochromatic contour obtained from the separated stress components which compares well with the analytical plot of $(\sigma_1 - \sigma_2)$ (Fig. 2a).

Performance of the Stress Separation Algorithm for Experimental Data

For the problem of disk under diametral compression, the experimental data of isoclinic is obtained using the plane polariscope based algorithm of Mangal and Ramesh [26] and fringe order is extracted using the six-step algorithm [27] based on circular polariscope arrangement. In order to study the influences of noise present in isochromatic / isoclinic data on separated stress components, the raw unwrapped experimental data is used initially for stress separation.

Figures 3a and 3b show the binary contours of isochromatics $(\sigma_1 - \sigma_2)$ and isoclinics (in steps of 10°) obtained using experimentally recorded phase shifted images. The choice of plotting binary contours is chosen as it is brought out in Part-A of the paper that a grey scale plot is deceptive in not reflecting the true quality of the photoelastic data visually. The individual stress components are obtained using the experimental data as mentioned in the previous section. Figs. 3c-e show the pseudo contours of σ_x, σ_y and τ_{xy} and Fig. 3f shows the isochromatic contour obtained using the separated stress components. Interestingly the $(\sigma_1 - \sigma_2)$ contours reconstructed from the separated stress components match well with the theory but the pseudo fringe contours of σ_x, σ_y and τ_{xy} show significant streaks. This problem needs to be addressed. To understand this phenomena, data for a line $y/R = 0.43$ is considered. This corresponds to the line 178 and the other lines required are, line 177 and 179 for stress separation.

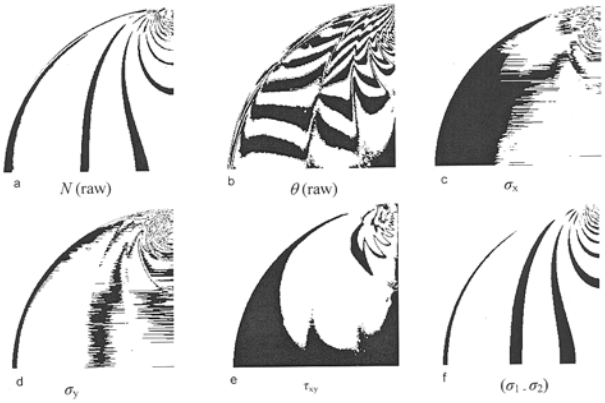

Fig.3

Pseudo fringe contours showing variation of stresses for a problem of disk under diametral compression determined by shear difference technique (using raw experimental data). (a) N (b) θ (isoclinic plot in steps of 10°) (c) σ_x (d) σ_y (e) τ_y (f) dark field isochromatic (using separated stress components)

Figure 4b shows the separated stress components in comparison to theory for the line 178. The jump in the stress values seen in Fig. 4b (line 178) causes a streak in

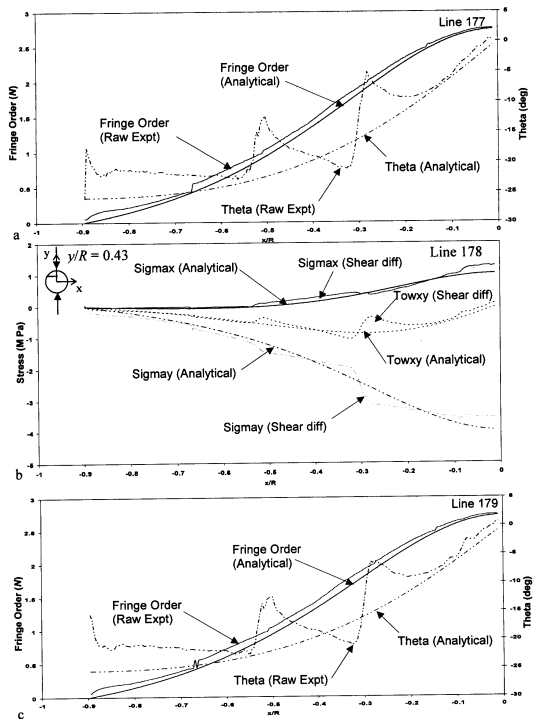

Fig.4

Quantitative plot (a) showing the variation of the fringe order and theta (raw experimental data) compared with the theoretical values along the line 177 (b) showing the variation of the individual stress values obtained using shear difference algorithm (using raw experimental data) compared with the theoretical stress values along the line 178 (y/R = 0.43) (c) showing the variation of the fringe order and theta (raw experimental data) compared with the theoretical values along the line 179.

the pseudo plot. When one calculates σ_x values along a line using the shear difference algorithm, one needs to calculate both the shear slope and the theta slope at every point of interest (See Eq. (4)). Fig. 4a shows the photoelastic data variation in the line above (line no. 177) and similarly Fig. 4c shows the photoelastic data variation in the line below (line no. 179). The isochromatic data is varying smoothly over both the lines (177 and 179). But whenever there is a jump in the isoclinic values, there is also a jump in the individual stress values (Fig. 4b). Thus, the undulation in the isoclinic data is the main reason for streak formation. This influences σ_x evaluation and subsequently the evaluation of σ_y.

Performance of the Stress Separartion Algorithm Using Smoothed Photoelastic Parameters

Figures 5a and 5b show the contours of smoothed isochromatics ($\sigma_1 - \sigma_2$) and isoclinics (in steps of 10°) obtained by employing the outlier algorithm [28]. Figs. 5c-e show the pseudo contours of σ_x , σ_y and τ_{xy} and Fig. 5f shows the isochromatic contour obtained using the separated stress components. Visually, a majority of the streaks are removed and only a few are present in the pseudo contours. Near the loading zones, there is some disturbance due to non-availability of good photoelastic data because of poor spatial resolution. Only σ_y pseudo contour has got a few problems on the top zone. Further in order to remove those few streaks, the stress values are again smoothed using the outlier algorithm with a span of thirty pixels and selecting a linear polynomial fitting for least squares analysis. Fig. 6 shows the Matlab plot of the whole field variation of smoothed individual stress components. One can observe a smooth variation of stress values over majority of the considered domain.

Handling of Model Domains with Generalized Boundaries

The problem of a ring subjected to internal pressure (Outer dia = 80mm, Inner dia = 40mm, thickness = 6 mm, Fsigma = 11.54 N/mm/fringe, load = 3.93 MPa) is chosen to illustrate this. Only one quarter of the ring is considered for evaluating the performance of the shear difference algorithm because of symmetry. The unwrapped isoclinic and isochromatic phasemaps are directly obtained from the work done in Part-A. At first, only the unwrapped isoclinic and isochromatic data directly obtained from the experiment is given as input for the shear difference algorithm. Fig. 7a and 7b show the contours of raw unwrapped isochromatics and isoclinics in steps of 10° obtained experimentally. It is to be noted that the starting and ending boundaries are both circular. The shear difference scheme is implemented in such a manner that for every starting boundary grid identified, the algorithm continues along a line until the penultimate pixel of that line. In the case of the final boundary pixel, the algorithm selects the ending boundary grid structure based on the pixel coordinates on adjacent lines. The shear difference equation for the ending grid is appropriately selected to complete the integration.

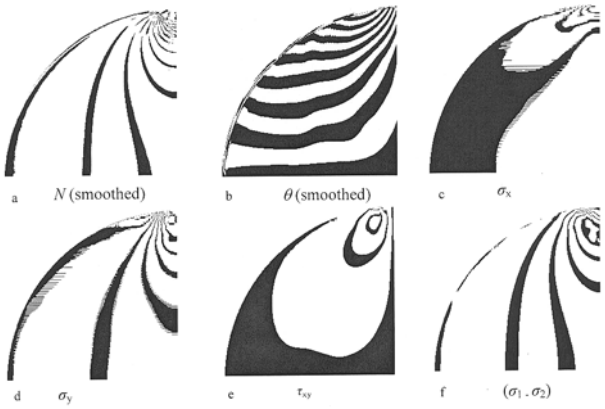

Fig.5

Pseudo fringe contours showing variation of stresses for a problem of disk under diametral compression determined by shear difference algorithm (using smoothed experimental data). (a) N (b) θ (isoclinic plot in steps of 10°) (c) σ_x (d) σ_y (e) τ_y (f) dark field isochromatic (using separated stress components)

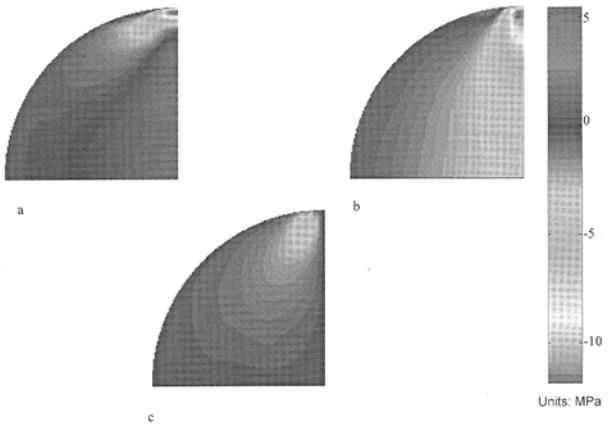

Fig.6

Matlab plot showing whole field variation of stresses for a problem of disk under diametral compression determined by shear difference technique (using smoothed experimental data). (a) σ_x (b) σ_y (c) τ_{xy}

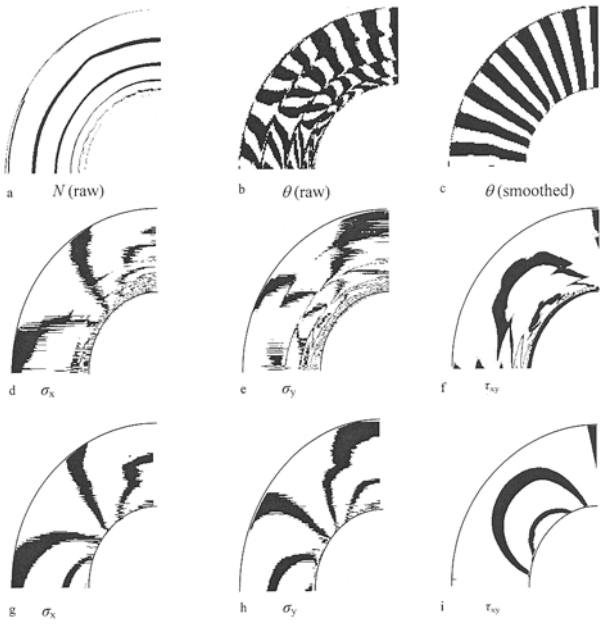

Fig.7

Pseudo fringe contours showing variation of stresses for a problem of ring subjected to internal pressure determined by shear difference algorithm (using raw and smoothed experimental data) along with the photoelastic parameter (N and θ (binary isoclinic plot in steps of 10°)

Figures 7d-f show the pseudo fringe contours of σ_x , σ_y and τ_{xy} obtained using the raw unwrapped experimental data. From these figures, one could clearly see the distorted pseudo fringe contours especially σ_y and τ_{xy}. It is shown in the previous section that smoothed photoelastic data especially that of isoclinics reduce the formation of streaks in the pseudo fringe contours. The smoothed photoelastic parameters are obtained using the outlier algorithm which is described in Part-A of the paper. As smoothing introduces only a marginal change on isochromatic data, it is not shown here pictorially. Fig. 7c shows the contours of isoclinics (in steps of 10°) obtained after smoothing.

Figures 7g-i show the pseudo fringe contours of σ_x , σ_y and τ_{xy} obtained using the smoothed photoelastic parameter. Majority of the streaks are removed and the pseudo fringe contours appear smooth. Only a small distortion is visible in the σ_x and σ_y pseudo fringe contours. Fig. 8 shows the Matlab plot of the whole field variation of individual stress components. One could observe a smooth variation in the whole field stress values over the domain considered.

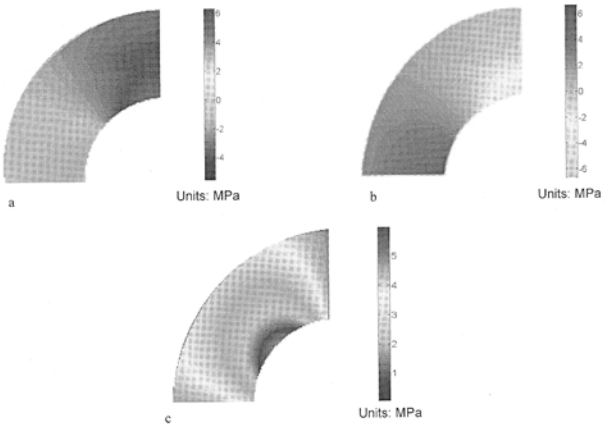

Fig.8

Matlab plot showing whole field variation of stresses for a problem of ring subjected to internal pressure determined by shear difference technique (using smoothed experimental data). (a) σ_x (b) σ_y (c) τ_{xy}

Conclusion

Digital implementation of the shear difference technique for whole field 2-D stress separation in photoelasticity has been proposed. A data structure for processing only the pixels within the model boundary is presented here. Various grid classifications to model a curved boundary for effecting stress separation by shear difference technique is presented. Initially the problem of a disk under diametral compression is solved and individual stress values are obtained. Recommendation for data smoothing especially of isoclinics is emphasized for the accurate evaluation of the separated stress values using the shear difference technique. Also smoothing of stress components is done for ensuring smooth variation of stress values. A new approach to represent whole field separated stress components in the form of pseudo fringe contours is presented. Finally, stress separation is done for the multiply connected model of a ring subjected to internal pressure. The methodology presented is easily extendable for evaluating separated stress components for stress frozen slices too.

References

1. Ramesh, K., "Digital Photoelasticity: Advanced Techniques and Application", Springer-Verlag, Berlin, Germany, 2000.

2. Haake, S. J. and Patterson, E. A., "The Determination of Principal Stresses from Photoelastic Data", Strain, Vol. 28, pp. 153-158, 1992.

3. Drucker, D. C., "Photoelastic Separation of Principal Stresses by Oblique Incidence", J. App. Mech., A156-A160, 1943.

4. Frocht, M. M., "Discussion of ref. [3]", J. App. Mech., 1944, A125-A126.

5. Brown, G. M. and Sullivan, J. L., "The Computer-aided Holophotoelastic Method", Exp. Mech., Vol. 30, No. 2, pp. 135-144, 1990.

6. Yoneyama, S., Morimoto, Y. and Kawamura, M., "Two-dimensional Stress Separation Using Phase-Stepping Interferometric Photoelasticity", Meas. Sci. Tech., Vol. 16, pp. 1329-1334, 2005.

7. Zhenkun, L., Hai, Y., Dazhen, Y. and Yilan, K., "Numerical Analysis Of Phase-stepping Interferometric Photoelasticity for Plane Stress Separation", Opt. and Lasers Eng., Vol. 45, No. 1, pp.77-82, 2007.

8. Barone, S. and Patterson, E. A., "Full Field Separation of Principal Stresses by Combined Thermo- and Photo-elasticity", Exp. Mech., Vol. 36, No. 4, pp.318-324, 1996.

9. Nurse, A. D., "Photoelastic Stress Separation Using Fast Fourier transforms", Proc. Int. Conf. Exp. Mech. (Ed. I.M. Allison), Oxford, 24th - 28th August, pp.559-562, 1998.

10. Ramesh, K. and Mangal, S. K., "Whole Field Stress Separation by Oblique Incidence Using Phase-shifting Technique", Proc. Int. Conf. Exp. Mech. (ICEM), Singapore, 29th November - 1st December, 2000.

11. Berghaus, D. G., "Combining Photoelasticity and Finite Element Method for Stress Analysis Using Least Squares", Exp. Mech., Vol. 31, pp. 36-41, 1991.

12. Mangal, S. K., Pathak, P. M., and Ramesh, K., "Use of Finite Element for Stress Separation in Digital Photoelasticity", J. Aero. Soc. India, Vol. 51, No. 4, pp. 205-213, 1999.

13. Umeagukwu, C., "Application of Photoelastic and Boundary Element Methods to Stress Analysis", Int. J. of Mech. Eng. Edu., Vol. 17, pp. 163-174, 1989.

14. Mitsui, Y. and Yoshida, S. Y., "Boundary Element Method Applied to Photoelastic Analysis", ASCE J. Eng. Mech, Vol. 109, pp. 619-631, 1983.

15. Chen, D., Becker, A. A., Jones, I. A., Hyde, T. H. and Wang, P., "Development of New Inverse Boundary Element Techniques in Photoelasticity", J. Strain Analysis for Eng. Des., Vol. 36, pp. 253-264, 2001.

16. Segerlind, L. J., "Stress-difference Elasticity and its Application to Photomechanics", Exp. Mech., Vol. 11, pp. 441-445, 1971.

17. Chandrashekhara, K. and Abraham Jacob, K., "An Experiment-numerical Hybrid Technique for Two-dimensional Stress Analysis", Strain, Vol. 13, pp. 25-31, 1977.

18. Quiroga, J. A. and Gonzalez-Cano, A., "Stress Separation from Photoelastic Data by a Multigrid Technique", Meas. Sci. Tech., Vol. 9, pp. 1204-1210, 1998.

19. Frocht, M. M., "Photoelasticity, Vol.1", John Wiley and Sons, Inc., NewYork, 1962.

20. Case, R. O. and Barkoff, A. C., "Computer-assisted Reduction of Two-dimensional Photoelastic Shear-Difference Data", Exp. Tech., pp. 32-37, 1986.

21. Trebuna F., "Some Problems of Accelerating the Measurements and Evaluating the Stress Fields by the Photostress Method", Exp. Tech., Vol. 14, pp. 36-40, 1990.

22. Haake, S. J., Patterson, E. A. and Wang, Z. F., "2D and 3D Separation of Stresses Using Automated Photoelasticity", Exp. Mech., Vol.36, No. 3, pp. 269-276, 1996.

23. Xue-Feng, Y., Long-Hui, J., Wei, X., Guan-Chang, J. and Hsien-Yang, Y., "Digital Shifting Photoelasticity with Optical Enlarged Unwrapping Technol-

ogy for Local Stress Measurement", Opt. and Lasers Tech., Vol. 37, No.7, pp. 582-589, 2005.

24. Patterson, E. A. and Wang, Z. F., "Towards Full-field Automated Photoelastic Analysis of Complex Components", Strain, Vol. 27, No. 2, pp. 49 - 56, 1990.

25. Vadovic, F., "Contribution to the Analysis of Errors in Photoelasticity", Exp. Mech., Vol. 5, No. 12, pp. 413-416, 1965.

26. Mangal S. K. and Ramesh. K., "Use of Multiple Loads to Extract Continuous Isoclinic Fringes by Phase-shifting", Strain, Vol. 35, No. 1, pp. 15-17, 1999 and its errata in Vol. 35, No. 2, pp. 76, 1999.

27. Ajovalasit, A., Barone, S., Petrucci, G., "A Method for Reducing the Influence of the Quarter Wave Plate Error in Phase Shifting Photoelasticity", J. Strain Analysis Eng. Des., Vol. 33, No. 3, pp. 207-216, 1998.

28. Math Works, Inc., "Curve Fitting Toolbox Ref. User's Guide", Math Works, Inc., Natick, MA, 2005.

29. Timoshenko, S. P. and Goodier, J. N., "Theory of Elasticity", McGraw - Hill, Singapore, 1987.

Appendix-A

Details of Digital Implementation

Figure A1 shows the various possible cases of boundaries that need to be considered for performing the shear difference integration. The various boundary types possible at the other end is exactly the mirror image of the various cases shown in Fig.A1. For any class of problem, one has to consider for each cases of the first, all the possible cases for the other boundary. For top-most and bottom-most row of pixel forming the model boundary, the integration has to be done differently (Figs.A1b and A1c).

The input for any problem consists of the *x* co-ordinate, the *y* co-ordinate, the fringe order (*N*) and the isoclinic parameter (θ) for each pixel in the domain of the problem under consideration. Special care needs to be

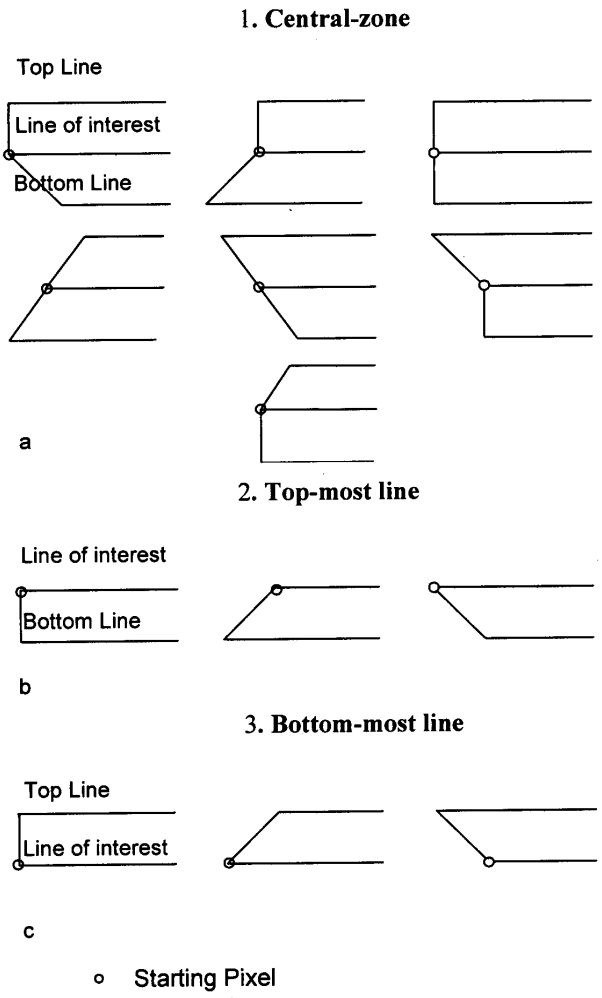

Fig.A1 Various cases of starting boundary grid in digital domain for horizontal scanning
(a) Central-zone (b) Top-most zone (c) Bottom-most zone

taken to delineate the problem domain and the background. The use of **.xbn* or **.ybn* file discussed in Part-A of the paper helps to identify the problem domain. In order to access data from any line of interest, the line number is stored in an array ny []. The starting boundary pixel number for each line in the model is stored in an array named tndp [] for correctly retrieving the boundary data value (Fig.A2). For proceeding along any line, the array 'tndp' is to be used in conjunction with the number of data points (ndp) in each line. These data along with the boundary information extracted from **.xbn* or **.ybn* are stored in a file with extension **.mbn*. Using the information in **.mbn*, the corresponding isochromatic and isoclinic values for all the points within the model domain are written row-wise in a file (**.shd*) along with the co-ordinates

Table-A1 : Modified boundary grid structure for digital implementation of shear difference technique

Boundary grids	Modified shear difference scheme
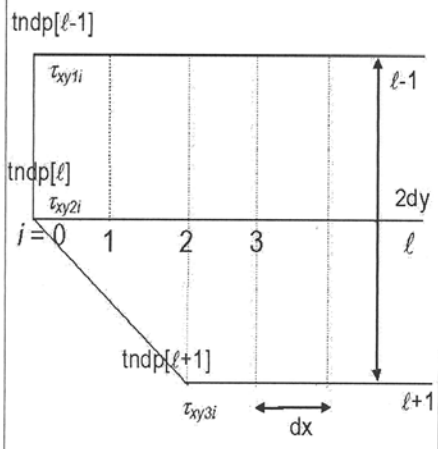	*i* is varying from 1 to 2 $\Delta\tau_{xy1i} = 0.5\left(N[tndp[\ell-1]+i]-N[tndp[\ell]+i]\right)(f_\sigma/h)$ $\sin 2\theta[tndp[\ell]+i])$ $\Delta\theta_{xy1i} = \left(\theta[tndp[\ell-1]+i]-\theta[tndp[\ell]+i]\right)$ $(f_\sigma/h)\cos 2\theta[tndp[\ell]+i])N[tndp[\ell]+i])$ $\sigma_{xi} = \sigma_{x(i-1)} - (\Delta\tau_{xy1i} + \Delta\theta_{xy1i})\frac{dx}{dy}$ $\sigma_{yi} = \sigma_{xi} - N[tndp[\ell]+i](f_\sigma/h)\cos(2\theta[tndp[\ell]+i])$ *i* >2 $k = nx1[l-1]-nx1[l+1]$ $\Delta\tau_{xy3i} = 0.5\left(N[tndp[\ell-1]+i]-N[tndp[\ell+1]+k+i]\right)$ $(f_\sigma/h)\sin 2\theta[tndp[\ell]+i])$ $\Delta\theta_{xy3i} = 0.5\left(\theta[tndp[\ell-1]+i]-\theta[tndp[\ell+1]+k+i]\right)$ $(f_\sigma/h)\cos 2\theta[tndp[\ell]+i])N[tndp[\ell]+i]$ $\sigma_{xi} = \sigma_{x(i-1)} - (\Delta\tau_{xy3i} + \Delta\theta_{xy3i})\frac{dx}{2dy}$ $\sigma_{yi} = \sigma_{xi} - N[tndp[\ell]+i](f_\sigma/h)\cos(2\theta[tndp[\ell]+i])$
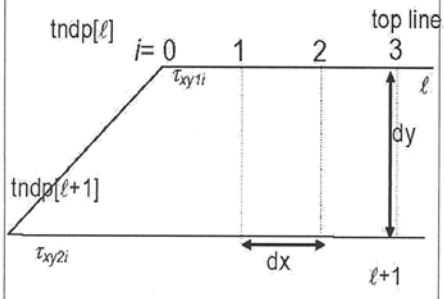	*i* is varying from 1 to number of data point on the line of interest (top line) $\Delta\tau_{xy1i} = 0.5\left(N[tndp[\ell]+i]-N[tndp[\ell+1]+nx1[l]-nx1[l+1]+i]\right)$ $(f_\sigma/h)\sin 2\theta[tndp[\ell]+i])$ $\Delta\theta_{xy1i} = \left(\theta[tndp[\ell]+i]-\theta[tndp[\ell+1]+nx1[l]-nx1[l+1]+i]\right)$ $(f_\sigma/h)\cos 2\theta[tndp[\ell]+i])N[tndp[\ell]+i])$ $\sigma_{xi} = \sigma_{x(i-1)} - (\Delta\tau_{xy1i} + \Delta\theta_{xy1i})\frac{dx}{dy}$ $\sigma_{yi} = \sigma_{xi} - N[tndp[\ell]+i](f_\sigma/h)\cos(2\theta[tndp[\ell]+i])$
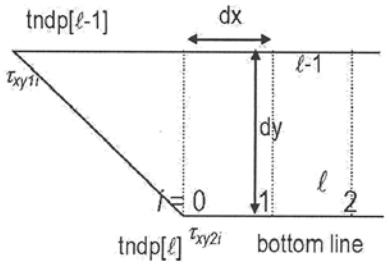	*i* is varying from 1 to number of data point on line of interest (bottom line) $\Delta\tau_{xy1i} = 0.5\left(N[tndp[\ell-1]+nx1[l]-nx1[l-1]+i]-N[tndp[\ell]+i]\right)$ $(f_\sigma/h)\sin 2\theta[tndp[\ell]+i])$ $\Delta\theta_{xy1i} = \left(\theta[tndp[\ell-1]+nx1[l]-nx1[l-1]+i]-\theta[tndp[\ell]+i]\right)$ $(f_\sigma/h)\cos 2\theta[tndp[\ell]+i])N[tndp[\ell]+i])$ $\sigma_{xi} = \sigma_{x(i-1)} - (\Delta\tau_{xy1i} + \Delta\theta_{xy1i})\frac{dx}{dy}$ $\sigma_{yi} = \sigma_{xi} - N[tndp[\ell]+i](f_\sigma/h)\cos(2\theta[tndp[\ell]+i])$

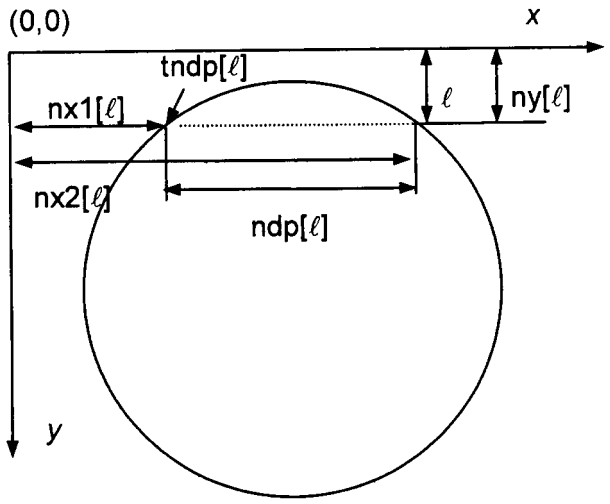

Fig.A2 : Figure showing the nomenclature of each term used in the algorithm

values. This helps to read the data for any three successive lines, at a time, from the whole data file.

Table-A1 shows the integration scheme that needs to be applied for a sample set of boundary grid classifications. Each point in the grid represents the centre of the pixel. In central zone (Fig.A1) three lines are available, however when the pixel position ('*i*') is varying from 0 to 2, only two grid lines are available and the shear difference scheme is modified accordingly. After the point 2, three lines are available and the equation as shown in Table-A1 are used. For the top-most and bottom-most zones, only two lines are available and an averaging scheme is done for stress separation as shown in Table-A1. In a similar manner, the integration scheme for every other boundary grid of Fig.A1 is developed. The modified grids discussed here can accommodate any type of boundary in digital domain and becomes useful for whole field stress separation.